JOURNAL OF Applied Polymer SCIENCE

Hydroxyl-Phosphazene-Wrapped Carbon Nanotubes and Its Application in Ethylene-Vinyl Acetate Copolymer

Tao Zhang, Zhongjie Du, Wei Zou, Hangquan Li, Chen Zhang
Key Laboratory of Carbon Fiber and Functional Polymers, Ministry of Education, Beijing University of Chemical Technology, Beijing 100029, China
Correspondence to: C. Zhang (E-mail: zhangch@mail.buct.edu.cn).

ABSTRACT: Multiwalled carbon nanotubes (MWNTs) are covalently grafted with hydroxyl modified phosphazene, which constitutes a novel flame retardant structure, and introduced into ethylene-vinyl acetate (EVA) copolymer via melt blending. The structure and morphology of the phosphazene-wrapped MWNTs are characterized using Fourier transform infrared spectroscopy and transmission electron microscopy. The grafted phosphazene introduces phosphorus- and nitrogen-containing species onto the surface of MWNTs and thus improves thermal stability of EVA resin and the dispersion of MWNTs in EVA matrix. Thermogravimetric analysis and cone calorimeter analysis reveal that phosphazene and MWNTs produce a synergistic effect on the enhancement of the thermal stability and flame retardancy of EVA. Furthermore, SEM observation indicates that phosphazene accelerates the formation of char residue on the surface of MWNTs. The char residue fills the space in the network structure of MWNTs and glues the MWNTs together. The dense char/MWNTs layers constitute a heat and mass block and therefore a better flame retardancy is observed. © 2013 Wiley Periodicals, Inc. J. Appl. Polym. Sci. 130: 4245–4254, 2013

KEYWORDS: nanotubes; graphene and fullerenes; flame retardance; thermal properties; composites

Received 26 February 2013; accepted 23 June 2013; Published online 16 July 2013
DOI: 10.1002/app.39706

INTRODUCTION

Carbon nanotubes (CNTs), due to their superior mechanical properties, excellent conductivity, and thermal stability, have been applied in various fields during the past two decades.[1] It has been considered a promising candidate for improving the mechanical or electrical properties of polymeric materials.[2–5] Recent years, the role of CNTs in the improvement of thermal stability and flame retardancy was reported.[6–11] It was considered that CNTs may form a barrier on the surface of the burning polymer and thus slowed down the degradation of the polymer matrix.

Kashiwagi et al.[12–16] reported that the formation of a continuous network of CNTs was critical for enhancing the flame retardancy of materials, for the network may act as a thermal shield to prevent energy feedback from the flame. To obtain a complete network, a good dispersion of CNTs was necessary. As a result, many efforts were devoted to surface modification of CNTs to improve their dispersion in polymer matrix.[17,18] Poly(acryloyl chloride) (PAC)-grafted multiwalled carbon nanotubes (MWNTs) was testified as an effective approach, and PAC could also introduce large amount of reactive groups on the surface of MWNTs, which was beneficial for further grafting other compounds.[19,20] Song et al.[21] and Ma et al.[22] fabricated a hybrid of MWNTs covalently wrapped with an intumescent flame retardant. The wrapped MWNTs could be easily dispersed in polymer matrix and enhanced flame retardancy and mechanical properties of the polymer matrix.

With increasing requirement of environmental protection, recent efforts on flame retarding were shifted toward to halogen-free systems.[23–28] Phosphazene-based flame retardants became more attractive for the researchers.[29–34] Cyclotriphosphazene, a ring compound consisting of alternating phosphorus and nitrogen atoms, exhibited unusual flame retardancy and self-extinguishing properties. During the combustion, the phosphazene decomposed itself and the phosphorus-containing species reacted with oxygen to generate phosphate derivatives, which could initiate the dehydration of polymer and catalyzed the formation of char residue. Simultaneously, the nitrogen-containing species might release NH_3 and nitric oxides, which not only brought away some heat, but also diluted the oxygen and flammable gas.[29–34] Moreover, the chlorine groups attached to the phosphorus atoms could be easily substituted by various nucleophiles leading to many different structures of phosphazene-based flame retardants. Wang and Qian synthesized epoxy functionalized phosphazene to improve the flame retardancy of epoxy resin.[32–34]

Ethylene-vinyl acetate (EVA) copolymer was one of the most widely used plastics in modern wire and cable industry, due to its desirable

physical and chemical properties and its easy acceptance of additives.[35] However, high flammability was one of its main drawbacks, which greatly restricted EVA from many applications. Consequently, improving the thermal stability and flame retardancy of EVA constituted one of the major interests in researches.[23–26,35,36]

In our previous works, the silica nanospheres, as a kind of inorganic oxides, were coated on the surface of MWNTs and formed a protective layer. The MWNTs/silica hybrids improved the thermal stability and flame retardancy of PMMA effectively.[37] Compared with the silica nanospheres, the modified phosphazene, as a rising organic flame retardant, could improve the thermal stability and flame retardant of EVA by itself. Meanwhile, the phosphazene could also generate some char residue on the surface of MWNTs to protect the MWNTs and fill the gap of the network of MWNTs to make it denser. Phosphazene and MWNTs could produce a synergistic effect on improving the thermal stability and flame retardant of EVA. In this article, a terminal hydroxyl-group phosphazene was synthesized and grafted onto acyl chloridized MWNTs, which was introduced into EVA as a flame retardant. It was expected that the grafting of phosphazene introduced phosphorus- and nitrogen-containing species onto the surface of MWNTs, imparting the latter good dispersion ability in the EVA matrix. The phosphazene also acted as a catalyst for the formation of char layer, which served as a block to protect the beneath materials.[21,22,37] The effect of the phosphazene-wrapped MWNTs on the thermal stability and flame retardancy of EVA was explored.

MATERIALS AND EXPERIMENTS

Materials

MWNTs (purity 95%, diameters 10–30 nm and length 0.5–500 μm) were provided by Shenzhen Nanotech Port Co. (China). Hexachlorocyclotriphosphazene ($N_3P_3Cl_6$) was purchased from Shanghai Jiachen Chemical Co. (China). Sodium hydride (NaH), sodium borohydride ($NaBH_4$), 4-hydroxybenzaldehyde, azobisisobutyronitrile (AIBN), acryloyl chloride, tetrahydrofuran (THF), 1,4-dioxane, ethyl acetate, ethanol, and methanol were purchased from Beijing Chemical Reagent Co. (China). EVA copolymer (EVA18-3), containing 18% of vinyl acetate with a melt index of 3.0 g/10 min at 190°C, was supplied by Beijing Eastern Petrochemical Co.

Synthesis of Hexakis(4-aldehydephenoxy)-Cyclotriphosphazene

A suspension of sodium 4-aldehydephenoxide in dry THF was prepared by mixing 27.4 g NaH (70 wt % diluted in oil) and a solution of 97.6 g 4-hydroxybenzaldehyde in 300 mL THF in a flask with mechanical stirring, reflux condensation, and nitrogen inlet.[34] Subsequently, 34.8 g $N_3P_3Cl_6$ was dissolved in 200 mL THF and was added dropwise to the flask over a period of 60 min, and then the reaction system was maintained at 65°C for 48 h. A light-brown powder denoted as hexakis (4-aldehydephenoxy)-cyclotriphosphazene (PN–CHO) was collected after recrystallization with ethyl acetate, and the yield was 76.5%.

Synthesis of Hexakis(4-hydroxyphenoxy)-Cyclotriphosphazene

$NaBH_4$ (5.6 g) was added to a reactor containing a solution of 20.0 g PN–CHO in 150 mL THF/methanol mixture.[34] The reaction system was stirred at room temperature for 24 h. A white powder denoted as hexakis (4-hydroxyphenoxy)-cyclotriphosphazene (PN–OH) was obtained after recrystallization with ethanol, and the yield was 85.7%.

Preparation of PAC-Grafted MWNTs

Pristine MWNTs 5.00 g were suspended and refluxed in a concentrated H_2SO_4/HNO_3 mixture (100 mL/100 mL) for 1 h at 140°C.[19,20,38] The acid-oxidized MWNTs were washed repeatedly with deionized water and dried in vacuum for 24 h at 60°C. Meanwhile, PAC was prepared via free radical polymerization of acryloyl chloride. In a 50-mL dry tube equipped with a magnetic stirring bar, a solution of 5.0 mL acryloyl chloride and 50 mg AIBN in 10.0 mL anhydrous 1,4-dioxane was stirred for 48 h at 60°C under N_2. The as-prepared PAC solution was directly added to a suspension of acid-oxidized MWNTs (5.0 g) in anhydrous 1,4-dioxane (150 mL), and then the mixtures were kept vigorous stirring at 80°C for 48 h. The black powder was collected and washed five times with dry THF. Afterward, PAC-*g*-MWNTs were obtained. All the procedures were carried out under N_2.

Preparation of PN–OH-Grafted MWNTs

A solution of 20.0 g PN–OH in 50 mL 1,4-dioxane was added dropwise to the suspension of 7.0 g PAC-*g*-MWNTs in 150 mL 1,4-dioxane with stirring at 60°C for 12 h. A black powder, denoted as PN-*g*-MWNTs, was collected by filtration and washed five times with dry THF. The synthesis procedure of PN-*g*-MWNTs was shown in Figure 1.

Preparation of EVA/MWNTs Composites

Pristine MWNTs and PN-*g*-MWNTs were separately blended with EVA in a HAAKE Polylab shear mixer at 160°C for 8 min with a rotating speed of 60 rpm. The composites were transferred to a mold and preheated at 180°C for 5 min, then pressed at 30 MPa for 10 min, and finally cool pressed for 20 min. The obtained EVA/MWNTs composites were denoted as EVA/pristine MWNTs and EVA/PN-*g*-MWNTs, respectively. The different concentrations of pristine MWNTs or PN-*g*-MWNTs in EVA composites were set at 2%, 4%, 6%, and 10%.

Characterization

Fourier transform infrared (FT-IR) spectrometer (Nicolet-Nexus 670) was used to detect the chemical structures of various samples, which was measured as a powder with potassium bromide. The morphologies of the MWNTs and the composites were observed by a transmission electron microscope (JEM100CX). The thermal stability was tested by thermogravimetric analysis (TGA, TA Instruments Q50), which were carried out from 40°C to 800°C at 10°C/min under N_2 atmosphere or air atmosphere. Ignition time (IT), heat release rate (HRR), and peak of heat release rate (PHRR) were determined using cone calorimeter (Cone, Fire Testing Technology), according to ISO 5660 at an external radiant heat flux of 50 kW/m^2. The samples for cone calorimeter test were 100 mm × 100 mm × 4 mm, and each sample retested three times. Scanning electron microscopy (SEM, Hitachi S4700) was used to observe the char residue of various EVA composites after cone calorimeter test.

RESULTS AND DISCUSSION

Structure and Morphology

The FT-IR spectra of PN–CHO and PN–OH were displayed in Figure 2. Both spectra had strong absorption peaks at 1266 cm^{-1}

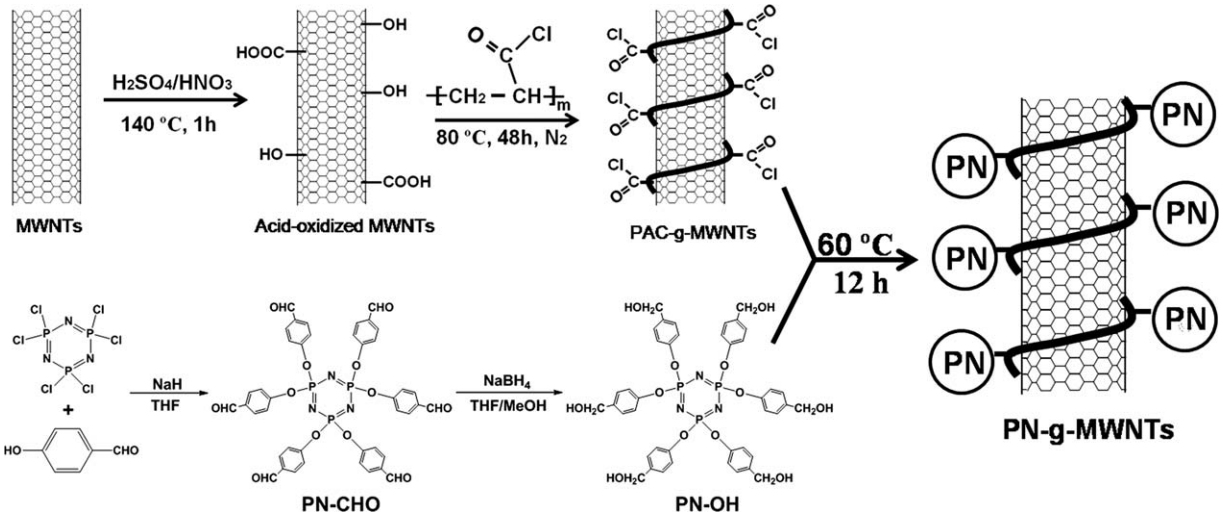

Figure 1. Schematic illustration of the synthesis procedure of PN-*g*-MWNTs.

and 1200 cm^{-1} corresponding to the P═N stretching vibration of phosphazene ring. The strong absorption peaks at 1176 cm^{-1} and 957 cm^{-1} revealed the presence of the phosphazene structure (P–O–C). The absorption peaks around 1580 cm^{-1} and 1495 cm^{-1} were attributed to the C═C stretching vibration of aromatic rings. However, there was an obvious difference between the spectra of PN–CHO [Figure 2(a)] and PN–OH [Figure 2(b)], where the absorption peak at 1702 cm^{-1}, indicated the presence of the aldehyde group (–CHO), was absent in the spectrum of PH–OH, and a broad absorption peak at 3400 cm^{-1} corresponding to the hydroxyl stretching (–OH) emerged.

Figure 3 was the FT-IR spectra for acid-oxidized MWNTs, PAC-*g*-MWNTs, and PN-*g*-MWNTs. In Figure 3(a), the broad peak at 3420 cm^{-1} was assigned to O-H stretching vibration in hydroxyl groups. In Figure 3(b), the strong absorption peaks at 1806 cm^{-1} and 1758 cm^{-1} were originated from characteristic C═O stretching vibration of acyl chloride. In Figure 3(c), the strong absorption peak at 1720 cm^{-1} was attributed to the stretching vibration of C═O in ester group, which indicated the reaction between PAC-*g*-MWNTs and PN–OH. Moreover, the absorption peaks at 1580 cm^{-1}, 1176 cm^{-1} and 957 cm^{-1} were coincident with the peaks of PN–OH [Figure 2(b)]. So it could be deduced that the PN–OH was covalently grafted onto the surface of MWNTs.

Transmission electron microscopy (TEM) was used to observe the morphologies of different MWNTs. It could be found that the diameters of pristine MWNTs were 20–30 nm and their surfaces seemed smooth and clear [Figure 4(a)]. After PAC grafting, however, the diameters increased to 40–50 nm, and the surfaces of PAC-*g*-MWNTs became rougher [Figure 4(b)]. Similarly, when PN–OH reacted with PAC-*g*-MWNTs [Figure 4(c,d)], the diameters of PN-*g*-MWNTs grew up to 60–70 nm. Therefore, the PN–OH-wrapped MWNTs (PN-*g*-MWNTs) were obtained.

Figure 5 showed the TGA traces of pristine MWNTs (a), PN–PAC (b), and PN-*g*-MWNTs (c), which were carried out from 40 to 800°C at 10°C/min under N_2 atmosphere. During the TGA test, pristine MWNTs presented good thermal stability (a), which had no weight loss before 800°C. To measure the content of PN–OH and PAC on the surface of MWNTs, a TGA sample named

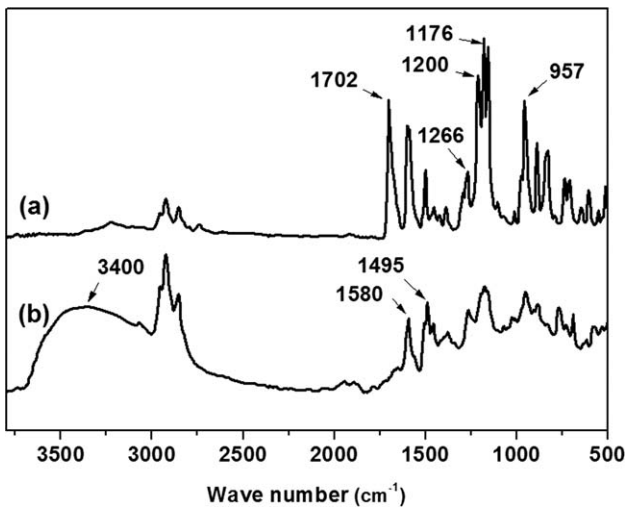

Figure 2. FT-IR spectra of PN–CHO (a) and PN–OH (b).

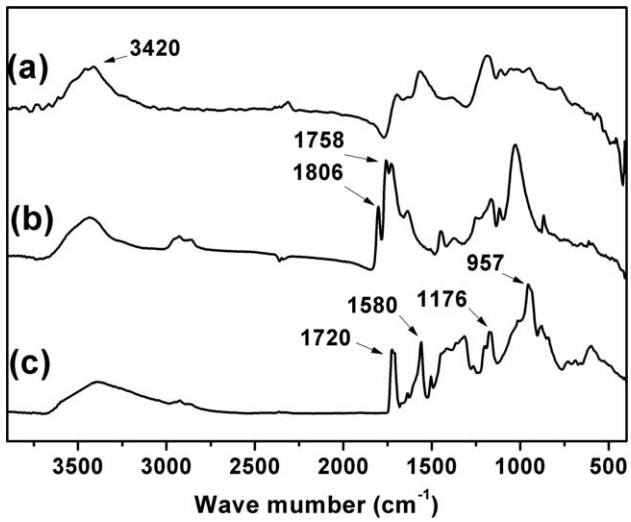

Figure 3. FT-IR spectra of acid-oxidized MWNTs (a), PAC-*g*-MWNTs (b), and PN-*g*-MWNTs (c).

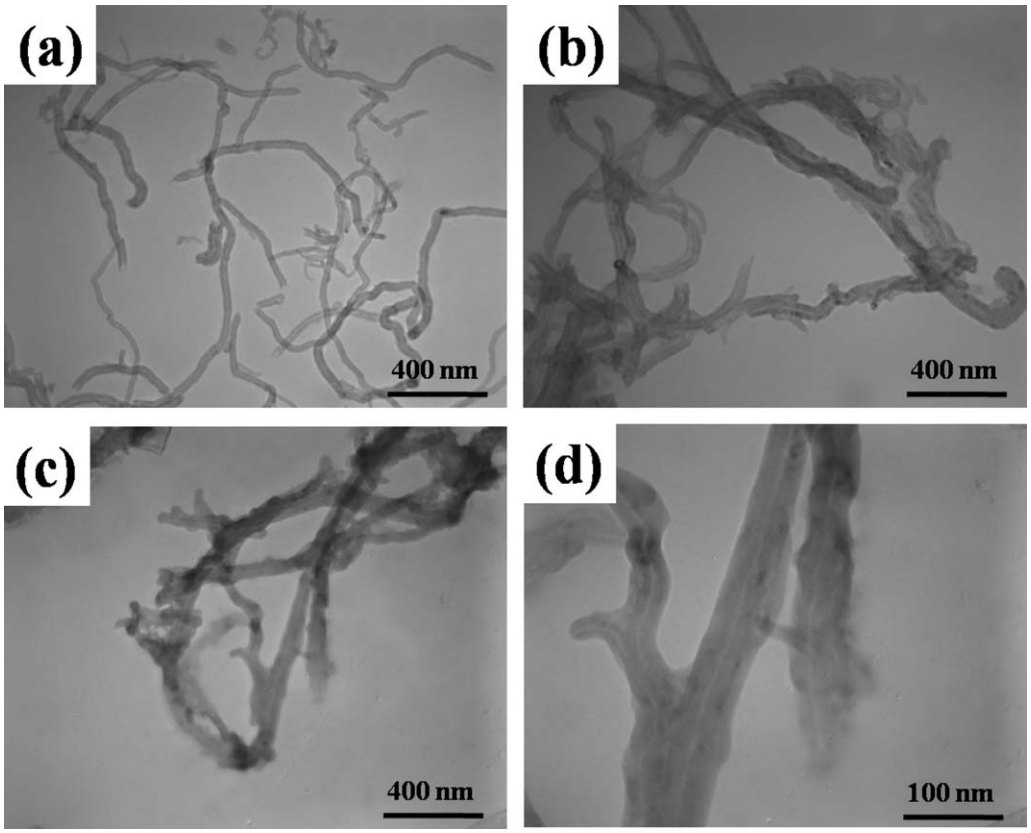

Figure 4. TEM images of pristine MWNTs (a), PAC-*g*-MWNTs (b), and PN-*g*-MWNTs (c and d).

PN–PAC was prepared by the reaction of PN–OH and PAC. The curve (b) reflected that the weight loss of PN–PAC was about 53.9% at 800°C. The curve (c) showed the weight loss of PN-*g*-MWNTs was about 35.9%, which was attributed to the degradation of PN–PAC. Therefore, according to the ratio of weight loss of curves (b) and (c), it could be figured out that the content of PN–PAC wrapped on the surface of MWNTs was about 66.7%.

Dispersion of MWNTs in EVA Composites

The TEM images of EVA composites presented the dispersion of MWNTs in Figure 6. Pristine MWNTs had some aggregations and entanglements in EVA matrix [Figure 6(a,b)], which was due to the poor compatibility between MWNTs and EVA matrix. After wrapped with PN–OH, however, PN-*g*-MWNTs dispersed in the EVA matrix homogeneously [Figure 6(c,d)], which profited from the similar polarities and ester groups between PN-*g*-MWNTs and EVA resin. Obviously, the surface modification was an effective method on improving the dispersion of MWNTs in polymer matrix.

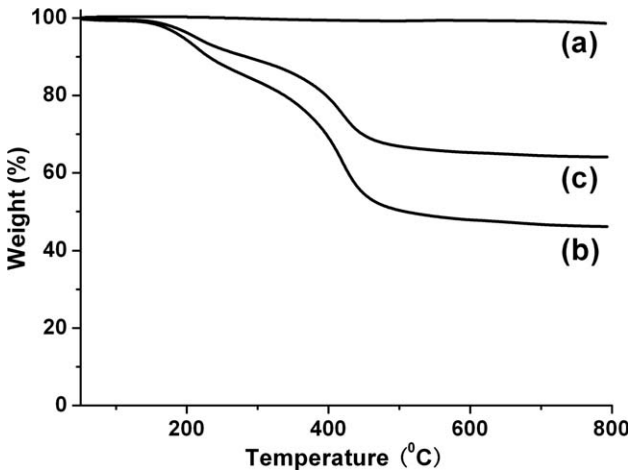

Figure 5. TGA curves of pristine MWNTs (a), PN–PAC (b), and PN-*g*-MWNTs (c) under N_2 atmosphere.

Thermal Stability of EVA Composites

The thermal stabilities of the different EVA composites were evaluated by TGA under air and N_2 atmospheres (Figures 7 and 8 and Table I). All of the TGA curves showed the thermal degradation of EVA underwent two main steps. The first degradation step corresponded to the deacylation reaction, which included the elimination of acetate side groups and the formation of unsaturated polymer backbone or polyene. Then the second step was associated with the chain scission of the unsaturated polymer backbone or polyene at higher temperatures.[34]

Under air atmosphere (Figure 7), the introduction of PN-*g*-MWNTs led to the thermal degradation shifting to higher temperatures, and the initial temperature of thermal degradation ($T_{5\%}$, the temperature at 5% weight loss occurred) increased from 326.0°C to 347.1°C (EVA/10% PN-*g*-MWNTs). In addition, compared with char residue of neat EVA, the char residue at 600°C increased with increasing concentration of PN-*g*-MWNTs, where the highest char residue of 12.1% (EVA/10% wt PN-*g*-MWNTs) was observed. It may be attributed to the combination of PN–OH and MWNTs. MWNTs could form a

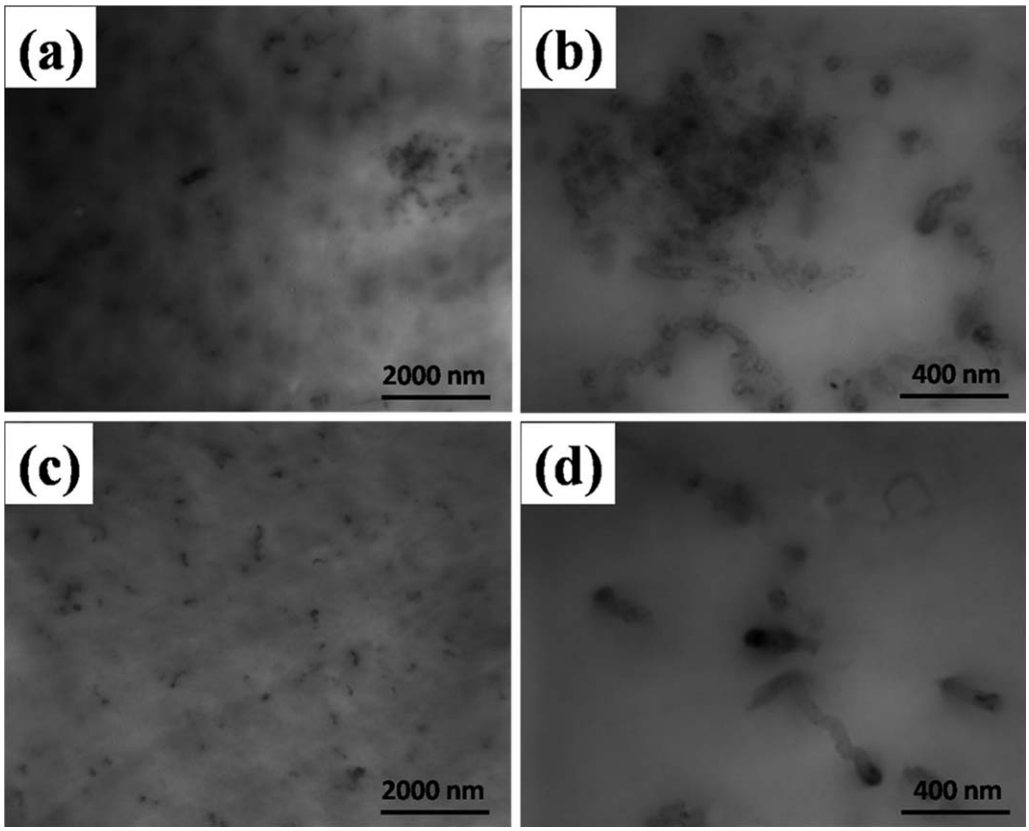

Figure 6. TEM images of different EVA composites: EVA/pristine MWNTs (a and b) and EVA/PN-*g*-MWNTs (c and d).

protective layer to block the heat flow and delay the degradation rate of EVA matrix.[13] On the other hand, the PN–OH decomposed itself and reacted with oxygen to generate some phosphate derivatives, which could catalyzed the formation of char residue and further delayed the thermal degradation of EVA matrix. It was worth mentioned that the char residue under N_2 atmosphere could reflect the fire behavior of the composites at certain extent (Figure 8). The char residue of EVA/PN-*g*-MWNTs composites under N_2 was 13.2% at 600°C, which exhibited a high ablative resistance. Therefore, the TGA tests indicated that the addition of PN-*g*-MWNTs promoted the production of the char residue and improved the thermal stability of EVA composites.

Flammability of EVA Composites

The flammability performances of EVA composites were measured by cone calorimeter. HRR curves of EVA/pristine MWNTs composites and EVA/PN-*g*-MWNTs composites and the corresponding parameters were presented in Figure 9 and Table II. Compared the IT of EVA composites, the introduction of

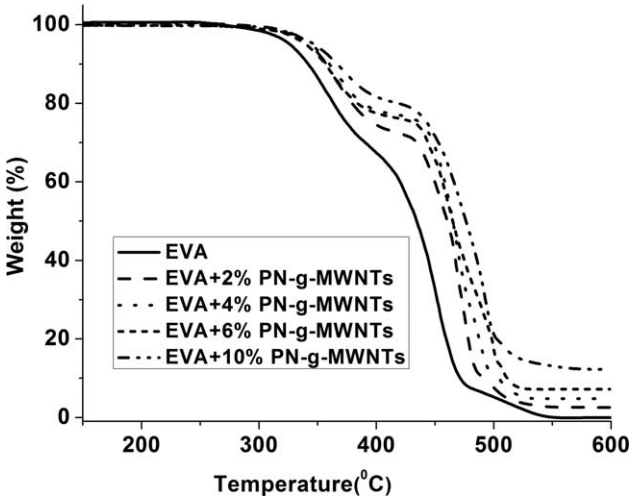

Figure 7. TGA curves of EVA and EVA composites under air atmospheres.

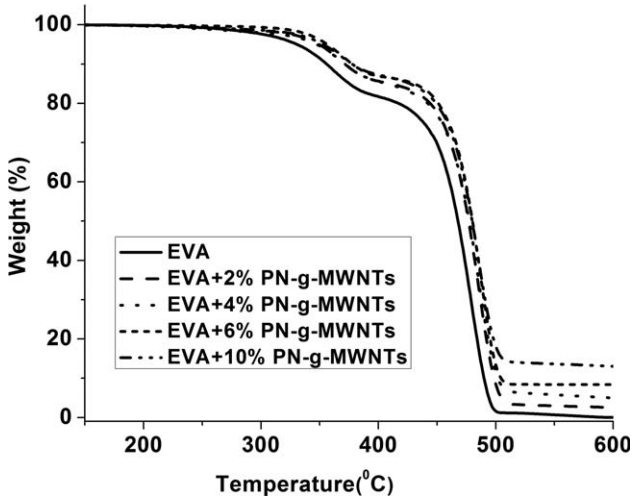

Figure 8. TGA curves of EVA and EVA composites under N_2 atmospheres.

Table I. DTG Results for EVA and EVA Composites Under Air and N_2 Atmospheres

	$T_{5\%}$ (°C)		T_{max1} (°C)		T_{max2} (°C)		Residue at 600°C (%)	
Sample ID	Air	N_2	Air	N_2	Air	N_2	Air	N_2
Neat EVA	326.0	334.9	352.5	360.3	452.3	477.1	0	0
EVA/2%PN-*g*-MWNTs	342.9	351.8	362.7	368.2	469.3	485.2	2.4	2.5
EVA/4%PN-*g*-MWNTs	343.1	352.1	366.5	368.3	477.2	485.7	4.8	5.3
EVA/6%PN-*g*-MWNTs	342.9	359.0	365.8	367.6	480.5	486.9	7.3	8.7
EVA/10%PN-*g*-MWNTs	347.1	358.0	369.8	369.5	488.7	486.2	12.1	13.2

$T_{5\%}$, the temperature at 5% weight loss occurred; T_{max1}, the temperature at the maximum weight loss rate of the first thermal degradation; and T_{max2}, the temperature at the maximum weight loss rate of the second thermal degradation.

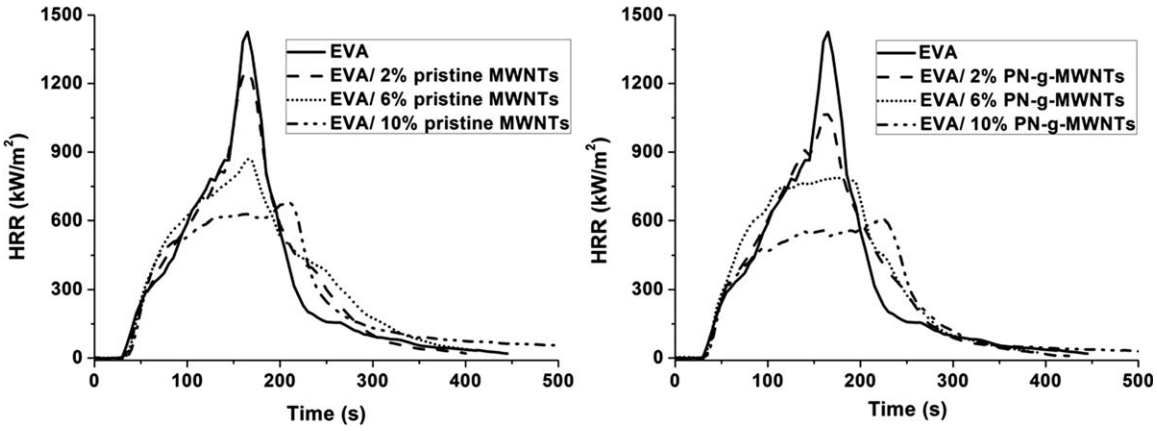

Figure 9. Heat release rate curves of EVA/pristine MWNTs (left) and EVA/PN-*g*-MWNTs (right).

pristine MWNTs did not affect the IT of EVA matrix, which was due to the competition between the effect of thermal conductivity and the shielding performance of external radiant flux.[13] The pristine MWNTs improved the thermal conductivity of EVA matrix. However, the molten EVA flowed easily under the external radiant flux, which was beneficial for pristine MWNTs to form the network on the surface of EVA and shielding the external radiant flux. Compared with the pristine MWNTs, the PN-*g*-MWNTs shorted the IT obviously, which was attributed to the catalysis of phosphorus- and nitrogen-containing species. As the existence of PN–OH, the IT of EVA/PN-*g*-MWNTs was shorter than that of EVA/pristine MWNTs.

After ignition, the neat EVA samples burned quickly with a sharp HRR curve appearing at 30–230 s, where the PHRR reached 1425 kW/m^2 at 165 s. The introduction of pristine MWNTs, however, delayed the quick combustion and reduced the PHRR, which was attributed to the formation of the network structure of MWNTs. The network structure acted as a protective shield to block the heat and mass exchange between

Table II. Cone Calorimeter Results for EVA and EVA Composites

Sample ID	IT (s)	T_{PHRR} (s)	PHRR (kW/m^2)	AHRR (kW/m^2)
Neat EVA	33 ± 1	165 ± 5	1425 ± 13	396 ± 7
EVA/2%pristine MWNTs	33 ± 1	165 ± 5	1266 ± 11	402 ± 3
EVA/6%pristine MWNTs	32 ± 2	165 ± 5	892 ± 15	387 ± 9
EVA/10%pristine MWNTs	34 ± 1	215 ± 5	678 ± 9	352 ± 6
EVA/2%PN-*g*-MWNTs	30 ± 2	165 ± 5	1078 ± 16	394 ± 4
EVA/6%PN-*g*-MWNTs	29 ± 3	175 ± 5	801 ± 23	382 ± 7
EVA/10%PN-*g*-MWNTs	33 ± 1	235 ± 5	623 ± 14	343 ± 6
EVA/10%PN	25 ± 2	195 ± 5	801 ± 20	376 ± 11

IT, ignition time; PHRR, peak of heat release rate; T_{PHRR}, time to PHRR; and AHRR, average heat release rate (0–360 s).

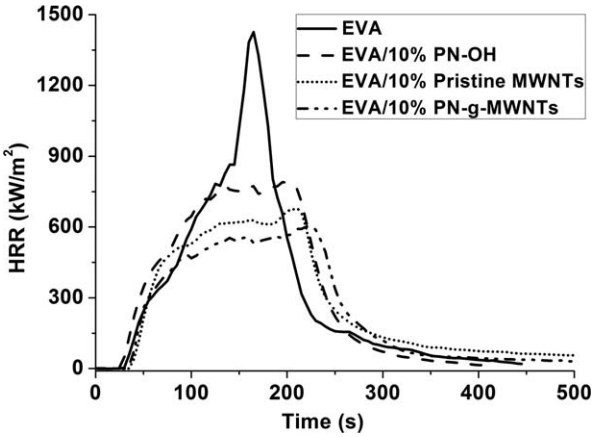

Figure 10. Effect of different flame retardants on HRR of EVA composites under the same concentration of 10%.

the inner and the outer of EVA composites. Moreover, with the concentration of pristine MWNTs increasing from 2% to 10%, the PHRR of EVA/MWNTs composites reduced from 1266 kW/m^2 to 678 kW/m^2 gradually (Table II). Compared with the pristine MWNTs, the PHRR of EVA/PN-*g*-MWNTs composites was lower than that of EVA/pristine-MWNTs composites at the same concentration (Table II), which profited from the introduction of PN–OH. The PN–OH could catalyze the formation of char residue and improve the dispersion of MWNTs in EVA matrix. In addition, with the increasing concentration of PN-*g*-MWNTs, the times to PHRR (T_{PHRR}) were prolonged form 165 s (2%) to 235 s (10%) gradually. Therefore, the char residue and the better dispersion were beneficial to the formation of network structured protective layer.

To verify whether there was a synergistic effect between the PN–OH and MWNTs. The HRR curves of different EVA composites were compared in Figure 10, where the introduction of PN–OH, pristine MWNTs, and PN-*g*-MWNTs was unified at 10%. The PHRR of the different EVA composites were 801 kW/m^2, 678 kW/m^2, and 623 kW/m^2, respectively. It is worth noting that the PN-*g*-MWNTs provided the largest reduction of the PHRR. It was deduced that there was a synergistic effect between the PN–OH and MWNTs.

The appearance of char residue after cone calorimeter test might explain the improvement of HRR among different EVA composites (Figure 11). During the cone calorimeter test, neat EVA was completely melted to liquid with a lot of bubbles and

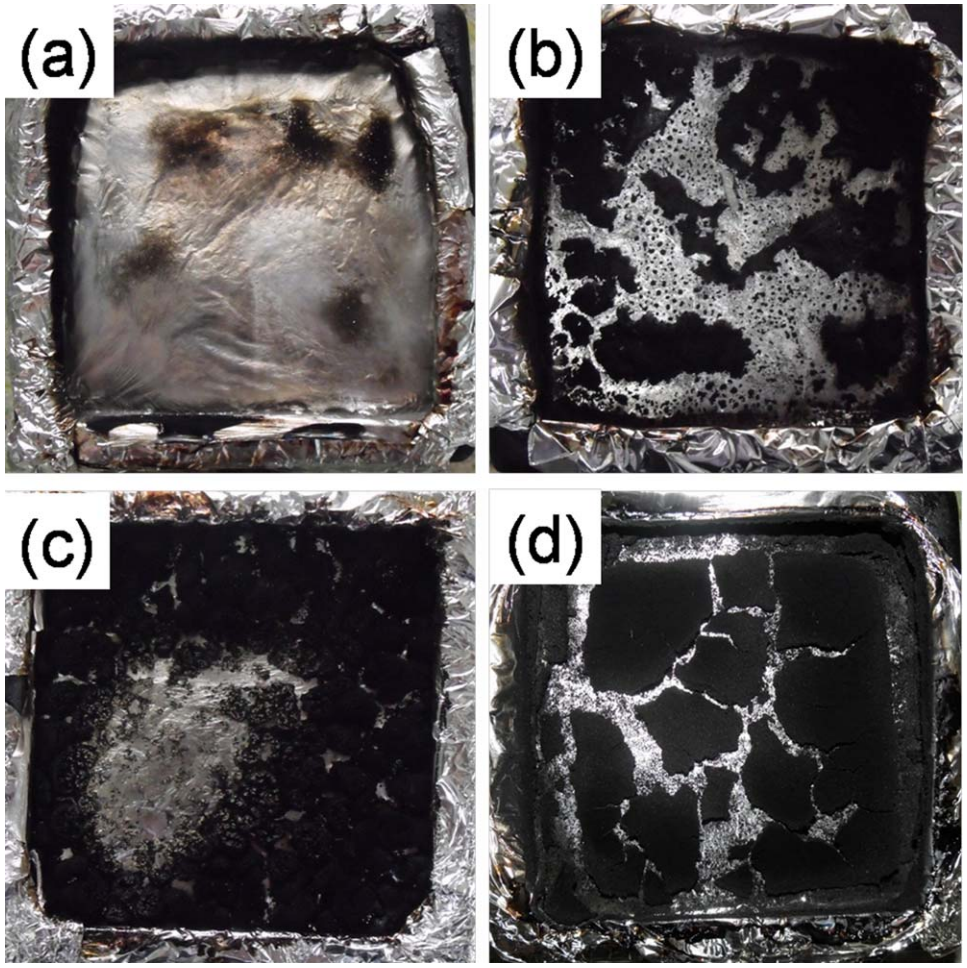

Figure 11. Photographs of the residue of EVA composites after cone calorimeter test: (a) EVA, (b) EVA/10% PN–CHO, (c) EVA/10% pristine MWNTs, and (d) EVA/10% PN-*g*-MWNTs. [Color figure can be viewed in the online issue, which is available at wileyonlinelibrary.com.]

burned dramatically. At the end of burning, there was no char residue left, as shown in Figure 11(a). The EVA/PN–OH composite had a similar phenomenon with that of neat EVA, but some char residue yielded at the bottom of the holder as shown in Figure 11(b), which came from the catalysis of phosphorus and nitrogen elements in PN–OH. Both EVA/pristine MWNTs composites [Figure 11(c)] and EVA/PN-*g*-MWNTs composites [Figure 11(d)] burned moderately and appeared some black spots on the surface of the burning samples, which was constructed by interlocked MWNTs. With the development of the combustion, these black spots became larger and joined together to form a continuous protective layer, which could prevent the exchange of heat and mass between the inner and outer of the burning samples. More importantly, EVA/PN-*g*-MWNTs generated more char residue than that of EVA/pristine MWNTs, which was ascribed to the catalysis of PN–OH. Compared the morphologies and strength of char residue, the char residue of EVA/PN-*g*-MWNTs was larger and stronger than that of EVA/pristine MWNTs. This proved that the char residue on the surface of MWNTs glued the latter together.

The char residue of EVA composites was further observed using SEM (Figure 12). Pristine MWNTs entangled together to form a continuous network. However, there were some small holes and

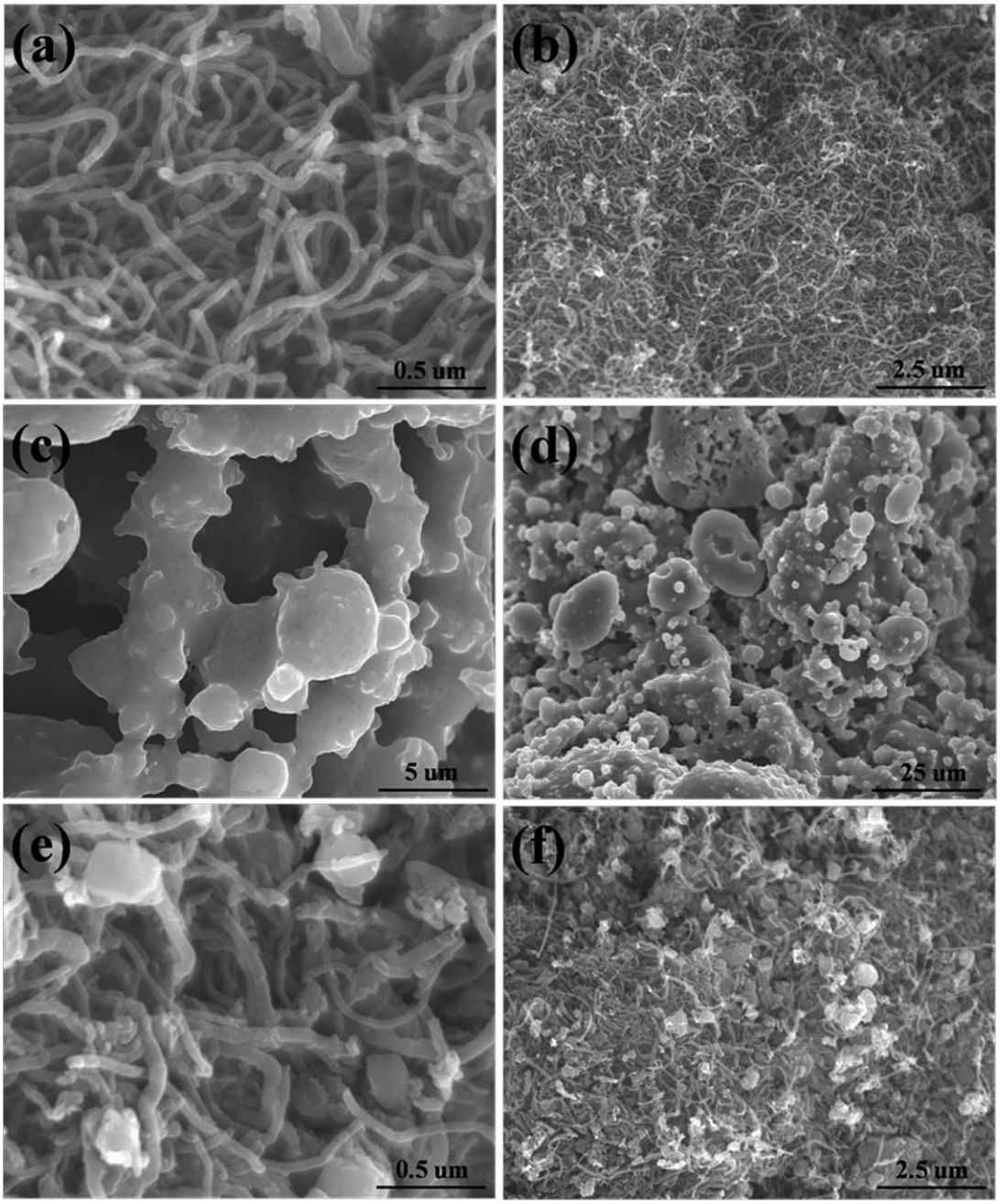

Figure 12. SEM images of the char residue of EVA composites after cone calorimeter test: EVA/pristine-MWNTs (a and b), EVA/PN–OH (c and d), and EVA/PN-*g*-MWNTs (e and f).

gaps in the network structure, which failed to completely block heat and mass [Figure 12(a,b)]. The PN–OH could catalyze EVA matrix to form char residue, but a continuous protective layer was still not observed [Figure 12(c,d)]. Only when the char residue covered the surface of MWNTs and glued them together, a complete network protective layer was obtained [Figure 12(e,f)]. According to the flame retardant mechanisms of phosphazene,[29–34] the PN–OH decomposed and generated char residue, which covered on the surface of MWNTs and protected the MWNTs. Simultaneously, some char residue filled into the gaps of the network structure and glued them together. On the other side, the MWNTs entangled and accumulated to form the network structure, which could enhance the strength of the char residue. With the increasing compactness of protective layer, more and more heat and mass were isolated. The HRR was further decreased and the flame retardancy of EVA was improved. Consequently, there was a synergistic effect between the PN–OH and MWNTs.

CONCLUSIONS

A hydroxyl group-modified phosphazene was synthesized and grafted onto acyl chloridized MWNTs leading to PN-*g*-MWNTs, which was introduced into EVA to enhance the flame retardancy and thermal stability. The introduced phosphorus- and nitrogen-containing species improved the dispersion of MWNTs. TGA tests indicated that PN-*g*-MWNTs increased the degradation temperature and enhanced the thermal stability of EVA obviously. During the combustion, the HRR reduced sharply with increasing concentration of PN-*g*-MWNTs. When the loading of PN-*g*-MWNTs was 10%, PHRR dropped from 1425 kW/m^2 to 623 kW/m^2. Comparing the morphologies of the char residue, the EVA/PN-*g*-MWNTs composites generated more char residue and formed a strong and dense protective layer, which was more effective to prevent the exchange of heat and mass. As a conclusion, PN-*g*-MWNTs improved the thermal stability and flame retardancy of EVA composites effectively.

ACKNOWLEDGMENTS

This work was supported by the 13th CHINA-JAPAN S & T Cooperation (2010DFA52070).

REFERENCES

1. Baughman, R. H.; Zakhidov, A. A.; de Heer, W. A. *Science* **2002**, *297*, 787.
2. Coleman, J. N.; Khan, U.; Blau, W. J.; Gunko, Y. K. *Carbon* **2006**, *44*, 1624.
3. Spitalsky, Z.; Tasis, D.; Papagelis, K.; Galiotis, C. *Prog. Polym. Sci.* **2010**, *35*, 357.
4. Fu, H.; Du, Z. J.; Zou, W.; Li, H. Q.; Zhang, C. *Mater. Lett.* **2012**, *78*, 54.
5. Hu, G. J.; Zhao, C. G.; Zhang, S. M. *Polymer* **2006**, *47*, 480.
6. Beyer, G. *Fire Mater.* **2002**, *26*, 291.
7. Schartel, B.; Potschke, P.; Knoll, U.; Abdel-Goad, M. *Eur. Polym. J.* **2005**, *41*, 1061.
8. Schartel, B.; Braun, U.; Knoll, U.; Bartholmai, M.; Goering, H.; Neubert, D.; Potschke, P. *Polym. Eng. Sci.* **2008**, *48*, 149.
9. Barus, S.; Zanetti, M.; Bracco, P.; Musso, S.; Chiodoni, A.; Tagliaferro, A. *Polym. Degrad. Stab.* **2010**, *95*, 756.
10. Yu, H. O.; Liu, J.; Wang, Z.; Jiang, Z. W.; Tang, T. *J. Phys. Chem. C* **2009**, *113*, 13092.
11. Yu, H. O.; Liu, J.; Wen, X.; Jiang, Z. W.; Wang, Y. J.; Wang, L.; Zheng, J.; Fu, S. Y.; Tang, T. *Polymer* **2011**, *52*, 4891.
12. Kashiwagi, T.; Du, F. M.; Winey, K. I.; Groth, K. M.; Shields, J. R.; Bellayer, S. P.; Kim, H.; Douglas, J. F. *Polymer* **2005**, *46*, 471.
13. Kashiwagi, T.; Grulke, E.; Hilding, J.; Groth, K.; Harris, R.; Butler, K.; Shields, J.; Kharchenko, S.; Douglas, J. *Polymer* **2004**, *45*, 4227.
14. Kashiwagi, T.; Fagan, J.; Douglas, J. F.; Yamamoto, K. *Polymer* **2007**, *48*, 4855.
15. Cipirano, B. H.; Kashiwagi, T.; Raghavan, S. R.; Yang, Y.; Grulke, E. A.; Yamamoto, K.; Shields, J. R.; Douglas, J. F. *Polymer* **2007**, *48*, 6086.
16. Kashiwagi, T.; Mu, M. F.; Winey, K.; Cipriano, B.; Raghavan, S. R.; Pack, S.; Rafailovich, M.; Yang, Y.; Grulke, E.; Shields, J.; Harris, R.; Douglas, J. *Polymer* **2008**, *49*, 4358.
17. Xie, X. L.; Mai, Y. W.; Zhou, X. P. *Mater. Sci. Eng. R* **2005**, *49*, 89.
18. Song, Y. S.; Youn, J. R. *Carbon* **2005**, *43*, 1378.
19. Wei, W.; Zhang, C.; Du, Z. J.; Liu, Y. X.; Li, C. J.; Li, H. Q. *Mater. Lett.* **2008**, *62*, 4167.
20. Liu, Y. X.; Du, Z. J.; Li, Y.; Zhang, C.; Li, C. J.; Yang, X. P.; Li, H. Q. *J. Polym. Sci. Part A* **2006**, *44*, 6880.
21. Song, P. A.; Xu, L. H.; Guo, Z. H.; Zhang, Y.; Fang, Z. P. *J. Mater. Chem.* **2008**, *18*, 5083.
22. Ma, H. Y.; Tong, L. F.; Xu, Z. B.; Fang, Z. P. *Adv. Funct. Mater.* **2008**, *18*, 414.
23. Bonnet, J.; Bounor-Legare, V.; Boisson, F.; Melis, F.; Gamino, G.; Cassagnau, P. *Polym. Degrad. Stab.* **2012**, *97*, 513.
24. Ye, L.; Qu, B. *J. Polym. Degrad. Stab.* **2008**, *93*, 918.
25. Alongi, J.; Poskovic, M.; Frache, A.; Trotta, F. *Polym. Degrad. Stab.* **2010**, *95*, 2093.
26. Liu, Y.; Zhang, Y.; Cao, Z. H.; Fang Z. P. *Ind. Eng. Chem. Res.* **2012**, *51*, 11059.
27. Chen, M. J.; Shao, Z. B.; Wang, X. L.; Chen, L.; Wang, Y. Z. *Ind. Eng. Chem. Res.* **2012**, *51*, 9769.
28. Wang, D. Y.; Song, Y. P.; Lin, L.; Wang, X. L.; Wang, Y. Z. A. *Polymer* **2011**, *52*, 233.
29. Zhang, T.; Cai, Q.; Wu, D. Z.; Jin, R. G. *J. Appl. Polym. Sci.* **2005**, *95*, 880.
30. Shan, X. Y.; Song, L.; Xing, W. Y.; Hu, Y.; Lo S. *Ind. Eng. Chem. Res.* **2012**, *51*, 13037.
31. Tao, K.; Li, J.; Xu, L.; Zhao, X. L.; Xue, L. X.; Fan, X. Y.; Yan, Q. *Polym. Degrad. Stab.* **2011**, *96*, 1248.
32. Liu, J.; Tang, J. Y.; Wang, X. D.; Wu, D. Z. *RSC Adv.* **2012**, *2*, 5789.

33. Qian, L. J.; Ye, R. J.; Qiu, Y.; Qu, S. R. *Polymer* **2011**, *52*, 5486.

34. Liu, R.; Wang, X. D. *Polym. Degrad. Stab.* **2009**, *94*, 617.

35. Yen, Y. Y.; Wang, H. T.; Guo, W. *J. Polym. Degrad. Stab.* **2012**, *97*, 863.

36. Allen, N. S.; Edge, M.; Rodriguez, M.; Liauw, C. M.; Fontan, E. *Polym. Degrad. Stab.* **2000**, *68*, 363.

37. Zhang, T.; Du, Z. J.; Zou, W.; Li, H. Q.; Zhang, C. *Polym. Degrad. Stab.* **2012**, *97*, 1716.

38. Liu, Y. X.; Zhang, C.; Du, Z. J.; Li, C. J.; Li, Y.; Li, H. Q.; Yang, X. P. *Carbon* **2008**, *46*, 1670.